Ultrasonics 75 (2017) 106–114

Contents lists available at ScienceDirect

Ultrasonics

journal homepage: www.elsevier.com/locate/ultras

Dynamic nonlinear focal shift in amplitude modulated moderately focused acoustic beams

Noé Jiménez [a], Francisco Camarena [b,*], Nuria González-Salido [c]

[a] Laboratoire d'Acoustique de l'Université du Maine, UMR CNRS 6613, Av. O. Messiaen, 72085 Le Mans, France
[b] Instituto de Instrumentación para Imagen Molecular (I3M), Centro Mixto UPV CSIC CIEMAT, Camino de Vera s/n, 46022 Valencia, Spain
[c] ITEFI, Spanish National Research Council (CSIC), Serrano 144, 28006 Madrid, Spain

ARTICLE INFO

Article history:
Received 15 September 2016
Received in revised form 24 November 2016
Accepted 26 November 2016
Available online 28 November 2016

2016 MSC:
00-01
99-00

Keywords:
Nonlinear acoustics
Acoustic radiation force
Biomedical ultrasound
Nonlinear focal shift
Finite-amplitude acoustic beams

ABSTRACT

The phenomenon of the displacement of the position of the pressure, intensity and acoustic radiation force maxima along the axis of focused acoustic beams under increasing driving amplitudes (nonlinear focal shift) is studied for the case of a moderately focused beam excited with continuous and 25 kHz amplitude modulated signals, both in water and tissue. We prove that in amplitude modulated beams the linear and nonlinear propagation effects coexist in a semi-period of modulation, giving place to a complex dynamic behavior, where the singular points of the beam (peak pressure, rarefaction, intensity and acoustic radiation force) locate at different points on axis as a function of time. These entire phenomena are explained in terms of harmonic generation and absorption during the propagation in a lossy nonlinear medium both for a continuous and an amplitude modulated beam. One of the possible applications of the acoustic radiation force displacement is the generation of shear waves at different locations by using a focused mono-element transducer excited by an amplitude modulated signal.

© 2016 Elsevier B.V. All rights reserved.

1. Introduction

The study of the acoustic field generated by focusing sources in the nonlinear regime is a continuously developing area of research as finite amplitude sound beams are increasingly used in medicine and industry [1–5]. Nonlinear propagation implies asymmetric wave steepening, progressive harmonic generation, nonlinear absorption, sound saturation, self-refraction and self-demodulation [6]. All these nonlinear effects change the spatial distribution of the acoustic field with respect to the linear case, i.e., among other things, the location of the on-axis peak compression and rarefaction pressure, intensity and acoustic radiation force (ARF), as well as the focal spot dimensions.

The nonlinear focal shift phenomenon, defined as the shift of the maximum pressure (and also intensity and ARF) position along the axis of focused acoustic beams under increasing driving voltages, has been discussed and interpreted in previous works. In 1980 Bakhvalov et al. [7] predicted a shift in the position of the on-axis pressure maximum in unfocused beams where a migration of the location of the maximum was shown, first away from, and then towards the transducer, as the exciting voltage of the source was increased. Duck and Starritt [3] (1986) studied this phenomenon in slightly focused sources, such as those used in commercial medical pulse-echo devices, showing that the nonlinear focal shift exists for on-axis maximum and negative pressure, with different behavior. Averkiou and Hamilton [8] (1997) observed this phenomenon experimentally in a moderately focused piston (linear gain $G = p/p_0 = 10.36$ with p is the value of the pressure at the geometrical focus and p_0 the pressure at the surface of the transducer). The nonlinear focal shift phenomenon was reported by Makov et al. [9] in low gain transducers, and discussed in terms of the harmonics nonlinearly generated during the propagation of a finite amplitude wave. They also provided experimental evidence of the nonlinear shift in slightly focused transducers ($G = 4$). Bessonova et al. [10] reported a numerical study which the nonlinear focal shift is shown for a moderately focused piston ($G = 10$) in a range of intensity covering both the shift of the maximum pressure towards the geometrical focus at first, even passing beyond the focus, and then the shift backwards to the transducer. They also provided an interpretation of the phenomenon based on the self-defocusing effect due to the asymmetrical distortion of the wave

* Corresponding author.
E-mail address: fracafe@fis.upv.es (F. Camarena).

http://dx.doi.org/10.1016/j.ultras.2016.11.021
0041-624X/© 2016 Elsevier B.V. All rights reserved.

profile and to the increase in propagation velocity of the compressive phase of the wave close to the beam axis. Recently, Camarena et al. [11] proved experimentally that at high amplitudes and for moderate focusing ($G = 18.8$) the position of the on-axis pressure maximum and radiation force maximum can surpass the geometrical focal length.

The location of the singular points of a focused ultrasonic beam, i.e., the on-axis maximum and negative pressure, maximum intensity and ARF, depends on the nonlinear degree of the propagated waves. This is especially relevant in moderately-focused beams since the focusing is high enough to make the nonlinear effects relevant, but at the same time the transversal area of the focus is not as small as in highly focused devices, making the self-refraction effect to play an important role [6,11]. The singular points of a beam (as for example the location of the maximum ARF) generated by a moderately focused mono-element emitter can be moved just by raising the amplitude of the voltage applied to the source. One of the applications that comes to mind is to generate a supersonic source of shear waves [12] with a focused mono-element transducer for elasticity imaging applications.

The adjustment of the focusing degree of the source and the modulation of the ultrasound amplitude are important tools that enable researchers to plan new treatments and monitoring, and consequently, the nonlinear shift effect must be taken into consideration. This is especially relevant in procedures that seek to reduce the degree of focusing of the ultrasonic source in order to increase the volume of the region treated, as it is in the case of ultrasonic-assisted blood-brain barrier opening techniques [13], which is particularly sensitive, taking into account that the frequencies used are lower than 500 kHz (making diffraction play a more important role) or in hyperthermia [14], if the whole tumor has to be sonicated. Also, monitoring procedures based on the modulation of the excitation amplitude of the emitter, such as HMI [15], should consider the nonlinear shift if at any time they reduce the focusing degree.

The aim of this work is to investigate experimentally and numerically the dynamic behavior of the singular points of a moderately focused beam operating from linear to nonlinear regime, and excited with amplitude modulated (AM) and continuous signals. Both water and soft tissue (human liver) media were considered. The paper is structured as follows: in Section 2 the experimental set-up and methods are described, providing a linear characterization of the beam and adjusting the source parameters to obtain the numerical results. Section 3 gives the experimental and numerical results for the maximum focal displacement in water (Section 3.1) and the dynamical focal shifts for a 25 kHz AM beam (Section 3.2). In Section 3.3 the study is numerically extended to propagation in soft tissue (human liver). Finally, the concluding remarks are given in Section 4.

2. Materials and methods

2.1. Experimental set-up

The experimental set-up for the pressure measurements in water follows the classical scheme of confronted emitting focused source and receiving calibrated membrane hydrophone, located inside a $0.75 \times 0.6 \times 0.5$ m water tank filled with degassed and distilled water at 26°, as shown in Fig. 1. The ultrasound source was formed by a plane single element piezoceramic crystal (PZ 26, Ferroperm Piezoceramics, Denmark) mounted in a custom designed stainless-steel housing and a poly-methyl methacrylate (PMMA) focusing lens with aperture $2a = 50$ mm and radius of curvature $R = 70$ mm. The resonant frequency of the transducer was $f_0 = 1.112$ MHz, and it was driven by a signal generator (14 bits, 100 MS/s, model PXI5412, National Instruments) and amplified by a linear RF amplifier (ENI 1040L, 400 W, +55 dB, ENI, Rochester, NY). The pressure field was measured by a PVDF membrane hydrophone with a 200 μm active diameter (149.6 mV/MPa sensitivity at 1.112 MHz, Model MHB-200, NTR/Onda) calibrated from 1 MHz to 20 MHz). The hydrophone signals were digitized at a sampling rate of 64 MHz by a digitizer (model PXI5620, National Instruments) averaged 500 times to increase the signal to noise ratio. An x-y-z micro-positioning system (OWIS GmbH) was used to move the hydrophone in three orthogonal directions with an accuracy of 10 μm. All the signal generation and acquisition process was based on a NI8176 National Instruments PXI-Technology controller, which also controlled the micro-positioning system. Temperature measurements were performed throughout the whole process to ensure no temperature changes of ±0.6 °C.

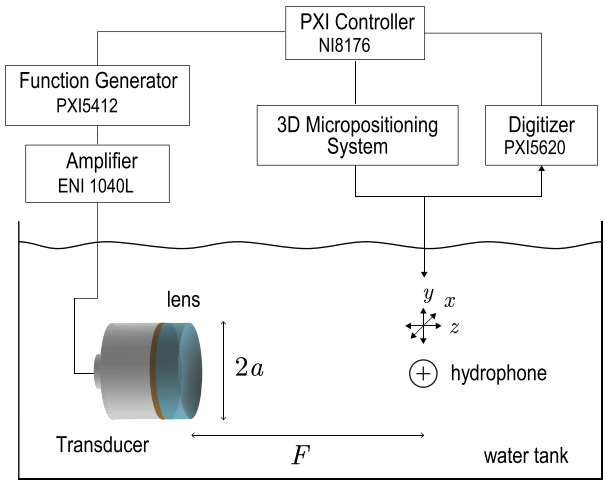


Fig. 1. Scheme of the experimental set-up for the pressure measurement in water.

2.2. Linear characterization of the beam

To accurately determinate the position of the radiator axis, a variant of the procedure described in Cathignol et al. [16] was developed. Firstly, the transducer was oriented along the z-axis of the micro-positioning system. In order to find the focal region of the transducer, the maximum pressure distribution generated by a 20-cycles sinusoidal pulsed burst was measured along the axis of the radiator. These measurements provided a rough estimation of the transducer focal area. Then, the pressure waveforms $p(t,x,y,z)$ were measured at the focal area in five planes along the z axis of the micro-positioning system, separated $\Delta z = 5$ mm. Waveforms were acquired along these planes in planes of 6 mm × 6 mm (x-y directions) at 0.5 mm spatial resolution (144 measurement points per plane). To avoid nonlinear effects in the propagation, low input voltage was employed ($V_0 = 6\ V_p$). Zero-gain band-pass filter was employed using an eight-order bandpass filter with cut-off frequencies $f_{low} = 0.91$ and $f_{high} = 1.31$ MHz to increase the signal-to-noise ratio and to avoid introducing any temporal delay in the signals. The maximum of each period of the 20-cycle tone burst was evaluated. The maximum of each waveform was then selected as the mean value of these 20 maxima. The equipressure curves in each plane built with the selected maxima typically had a circular form: This was indicative of the good axial symmetry of the radiator. Finally, the coordinates (x-y) of the maximum and the z position of each transversal plane were used for fitting a 3D line that determines the acoustic axis.

A set of 63 signals was measured on the previously determined radiator axis (dots in Fig. 2) using an input voltage at the trans-

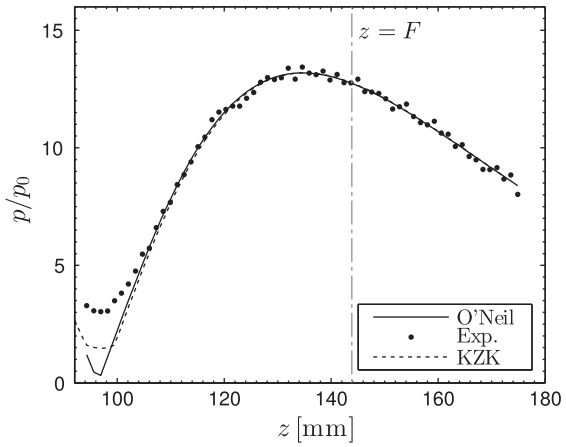


Fig. 2. On-axis maximum pressure distribution for small amplitude wave propagation obtained by experimental data (dots), O'Neill solution (solid line) and KZK numerical solution (dotted line). The vertical dashed-dotted line shows the position of the geometric focus.

ducer of $V_0 = 6\ V_p$. Time of flight (t_f) was estimated at each point on the axis to locate the absolute hydrophone position (z_0') with respect to the radiator. The time of flight was determined as the time elapsed until the signal energy of the wave packet reaches 5% of its maximum. A linear fit was then performed to estimate the source off-set distance relative to the 3D positioning system. It was fitted as $z' = c_0 t_f + z_0'$, where z' was the axial position of the different points, c_0 the estimated speed of sound in pure water. The least squares error for this fit ensures that accuracy is better than ±0.7 mm for absolute focal estimations.

The geometrical focal length (considering the PMMA focusing lens) and the aperture of the transducer were nominally rated by the manufacturer as $F = 157$ mm and $2a = 50$ mm, respectively. The fit of the analytic O'Neil solution [17] to the experimental data is shown in Fig. 2 and provides an effective aperture of the transducer of 55 mm and an effective geometrical focal length of 143.9 mm. Finally, KZK simulations [18] were performed for various values of the focal and source aperture to obtain the "best fit" with the experimental measurements in the focal zone at low amplitude [19], providing an effective aperture and geometrical focal length of $2a = 56$ mm and $F = 143.9$ mm respectively. These geometrical parameters lead to a linear gain of $G = 12.79$. The pressure amplitude of the signal at the geometric focus, $p_F = 40.4$ kPa, was determined for an input voltage excitation of $6\ V_p$. The signal spectrum was corrected using the hydrophone sensitivity over the frequency range from 1 MHz to 20 MHz. The relation between the pressure at the transducer face, p_0, and the pressure at the geometrical focus is given by $p_0 = p_F/G = 3.16$ kPa. For other source amplitudes, the source pressure amplitude was assumed to be linearly proportional to the driving voltage to the source [19].

The results of both the O'Neil model and the one calculated with the "best fit" aperture and geometrical focal length in the KZK simulation, are in good agreement with the experimental data, as shown in Fig. 2. The peak pressure location in linear regime is located at $z = 135.6$ mm, which corresponds to a linear focal shift of $\Delta F = -8.6$ mm, with respect to the geometric focus. This initial shift is used to obtain the focal shifts in nonlinear regime.

2.3. Measurement procedure

To study the nonlinear focal shift produced by continuous and AM beams, the acoustic field on the radiator axis was measured for different initial pressures. Firstly, the transducer was excited by a 40 cycles-sine wave burst with 27 values of amplitude with voltages ranging from 5 V_p to 228 V_p (assuming a source pressure amplitude linearly proportional to the driving voltage from $p_0 = 2.63$ kPa to $p_0 = 120$ kPa). Then, the experiment was repeated for an AM beam generated by the 25 kHz modulation of a continuous beam (90 cycles-sine wave burst). For all the input voltages, the axial field generated was measured at 63 points on the radiator axis with a spatial resolution of 1.3 mm in order to evaluate the position of the on-axis pressure maximum with an accuracy sensitive to the nonlinear pressure focal shift phenomenon (estimated as less than 1 cm from the numerical simulations [9]).

The on-axis intensity distribution, $I(z)$, was evaluated using the temporal pressure waveforms $p(t,z)$ as:

$$I(z) = \frac{1}{nT}\int_{t_0}^{t_0+nT} \frac{p^2(z,t)}{\rho_0 c_0} dt, \tag{1}$$

where T is the period, n an integer, ρ_0 the ambient density and c_0 the sound speed.

As the transversal dimension of the beam is much smaller than the characteristic absorption length, the transversal component of the ARF in the focal area is practically negligible [20,21]. Therefore the axial component of the ARF in a viscous heat-conducting medium can be evaluated from [22]:

$$\mathrm{ARF}_z(z) = \frac{b}{\rho_0^3 c_0^5}\left\langle \left(\frac{\partial p(t,z)}{\partial t}\right)^2 \right\rangle, \tag{2}$$

where b is the effective dissipation $b = \xi + 4\eta/3 + \chi(1/C_v + 1/C_p)$ with ξ and η the bulk and shear viscosities respectively, χ the thermal conductivity and C_v and C_p are the heat capacities of the medium at constant volume and pressure, respectively. The angular brackets denote temporal averaging over fast acoustic oscillations. This equation, for a monochromatic wave reduces to

$$\mathrm{ARF}_z(z) = 2\alpha \frac{I(z)}{c_0}, \tag{3}$$

where $\alpha = b\omega^2/2\rho_0 c_0^3$ is the medium attenuation coefficient at frequency ω and I the intensity of the spectral component. Alternatively, Eq. (3) can be derived by perturbation methods and the ARF is equal to the gradient of the acoustic energy density [23]. If the attenuation coefficient shows a power-law dependence on frequency, as observed in soft-tissues, the axial component of the ARF in the equivalent fluid is calculated as the sum of the acoustic radiation forces produced by each spectral component as:

$$\mathrm{ARF}_z(z) = \frac{2}{c_0}\sum_{n=1}^{\infty} \alpha_0 (n\omega_0)^\gamma I_n(z), \tag{4}$$

where the frequency dependent attenuation is given by $\alpha(\omega) = \alpha_0 \omega^\gamma$, with α_0 the power law pre-factor in $\mathrm{Np(rad/s)}^{-\gamma}\,\mathrm{m}^{-1}$ units, γ the exponent of the frequency power law and $I_n(z)$ the intensity field of the n-th spectral component. This relation must be corrected by a term $c_0^{-2}\partial I/\partial t$ accounting for the temporal modulation of the signal [24], but in this study due to the different order of magnitude of the carrier and modulation frequencies, this term can be neglected. This is also supported by the experimental and numerical results in Section 3. The validity of this relation is restricted at the focus of moderately focused beams, where the waves can be considered quasi-planes. It is worth noting here that Eqs. (2) and (4) are equivalent for $\gamma = 2$.

Finally, to obtain the experimental focal displacements, the axial distributions of peak positive/negative pressure, intensity and ARF curves were fitted to a polynomial of degree four over the focal area. The estimated position of the maxima provides the absolute focal displacements, where the errors committed

are mainly due to the uncertainty in the time of flight technique, and are below ±1 mm for all the cases shown.

2.4. Numerical model

Numerical modeling of the experimental conditions was performed by using the numerical solution of the KZK nonlinear parabolic equation over a cylindrical axisymmetric coordinate system $\mathbf{r}(r,z)$. This model takes into account the nonlinearity, diffraction (assuming a beam in the paraxial/parabolic approximation), thermo-viscous absorption and relaxation [6].

For propagation along the positive z-axis, the dimensionless KZK equation in a thermoviscous and relaxing media is written as [18,25]

$$\frac{\partial P}{\partial \sigma}=\frac{1}{4G}\int_{-\infty}^{\tau}\left(\frac{\partial^2 P}{\partial \rho^2}+\frac{1}{\rho}\frac{\partial P}{\partial \rho}\right)d\tau+A\frac{\partial^2 P}{\partial \tau^2}+NP\frac{\partial P}{\partial \tau}+\sum_n D_n\int_{-\infty}^{\tau}\times\frac{\partial^2 P}{\partial \tau'^2}e^{-(\tau-\tau')/\theta_n}d\tau', \tag{5}$$

where $P=p/p_0$ is the pressure normalized to the pressure at the source plane $p_0, \sigma=z/F$ the dimensionless axial coordinate with F the source geometric focal, $\rho=r/a$ the dimensionless radial coordinate with a the source radius, $\tau=\omega_0 t'$ the dimensionless retarded time with ω_0 the beam angular frequency, $t'=t-z/c_0$ the retarded time, $G=z_d/F$ the gain with $z_d=\omega_0 a^2/2c_0$ the characteristic diffraction distance (i.e. the Rayleigh distance), $A=F/z_a$ the absorption parameter with $z_a=1/\alpha$ the characteristic absorption distance and $\alpha=b\omega_0^2/2rho_0c_0^3$ the thermoviscous absorption coefficient, $N=F/z_s$ the parameter of nonlinearity with $z_s=\rho_0c_0^3/\beta p_0\omega_0$ the shock formation distance for a plane-wave, and β the coefficient of nonlinearity of the medium. The relaxation parameters are $\theta_n=\omega_0 t_n$ and $D_n=k_0Fc_n'/c_0$, where t_n and c_n' are the characteristic relaxation time and the small-signal sound speed increment for the n-th relaxation process, respectively.

For simulations in water, i.e., thermo-viscous fluids, Eq. (5) was solved using the time-domain algorithm developed by Lee [18], the so called KZK-Texas code, and relaxation was neglected. For simulations in liver, i.e., frequency power-law attenuation media, Eq. (5) was solved numerically using the KZK-Texas code including multiple relaxation and heterogeneities in an axisymmetric domain [25]. The relaxation parameters were optimized to fit the tissue frequency dependent attenuation and dispersion [25], i.e., a frequency power-law attenuation and its corresponding dispersion. Three relaxation processes were used. Both numerical approaches were based on operator splitting, where each term was solved sequentially for each $\Delta\sigma$ step. Thus, the diffraction term, i.e., first right hand side term in Eq. (5), was solved using an implicit backward finite difference (IBFD) method for $\sigma<0.1$ and a Crank-Nicolson finite difference (CNFD) method thereafter. The same methods were used for the thermo-viscous absorption and relaxation terms, i.e., second and fourth RHS terms in Eq. (5). Finally, the nonlinearity, i.e., third RHS term in Eq. (5) was solved analytically using the Poisson solution, where it was checked that the nonlinear distortion would not allow the wave form to become multivalued. The $\Delta\sigma$ step was decreased accordingly to avoid multivalued waveforms. Finally, heterogeneities were included according to Ref. [25] Eq. (15) by a plane wave pressure transmission coefficient and a temporal phase shift in the retarded frame, accounting for the propagation through layers with different densities and speeds of sound.

Simulations were performed in water and tissue with both continuous and amplitude modulated beams. Seventy values of p_0 were used in each case, ranging from 5 kPa to 120 kPa to cover a similar range as in the measurements. Simulation parameters for water were $c_0=1488$ m/s, $\rho_0=998$ kg/m^3, $\beta=3.5, b=3.8$ mPa·s, $F=143.9$ mm and $a=28$ mm. These parameters lead to the dimensionless factors $G=12.79, A=4.1\cdot10^{-3}$, and the parameter of nonlinearity ranging between $5.24\cdot10^{-3}<N<0.128$. Therefore, the Gol'dberg ratio, $\Gamma=z_a/z_s=N/A$, ranges between $1.3<\Gamma<31.3$, so nonlinearity dominates over absorption effects. On the other hand, the Khokhlov number, $K=z_s/z_d=1/NG$, ranges between $14.6>K>0.6$, so the nonlinearity dominates over diffraction effects only for high amplitudes. In the case of simulations including tissue, a layer of liver tissue was introduced at $z=70$ mm. The parameters were $c_{liv}=1600, \rho_{liv}=1060$ and $\beta=4.35$; where the parameters of 3 relaxation processes were optimized to model a frequency power law attenuation $\alpha=\alpha_0\omega^\gamma$ with $\alpha=0.5$ dB/cm/MHz$^\gamma$ and $\gamma=1.1$. Both the retrieved attenuation and its corresponding dispersion using relaxation agrees with the frequency power-law from 0.5 to 40 MHz.

The source condition was modeled by applying a temporal delay across the source to account for the focusing as:

$$P(\tau,\rho)|_{\sigma=0}=p_s(\tau+G\rho^2)g(\rho), \tag{6}$$

where p_s is the temporal waveform and, for a uniform piston, $g(\rho)$ is the step function defined as $g(\rho)=1$ for $0\leqslant\rho\leqslant1$, and $g(\rho)=0$ for $\rho>1$.

For the continuous acoustic beam, the temporal waveform was expressed as

$$p_s(t)=p_0e^{-\left(\frac{\omega_0 t}{M\pi}\right)^m}\sin(\omega_0 t). \tag{7}$$

where the power m was chosen to simulate a nearly rectangular pulse with continuous amplitude, and the denominator M indicates the number of cycles simulated. Here $m=8$ and $M=25$ were used.

In the case of AM beams, the temporal waveform used was

$$p_s(t)=p_0e^{-\left(\frac{\omega_0 t}{\omega_0/\omega_m\pi}\right)^m}\sin(\omega_0 t)\sin(\omega_m t). \tag{8}$$

Here, we simulated only four AM packets, i.e. only 2 cycles of the modulation frequency, $f_m=\omega_m/2\pi=25$ kHz.

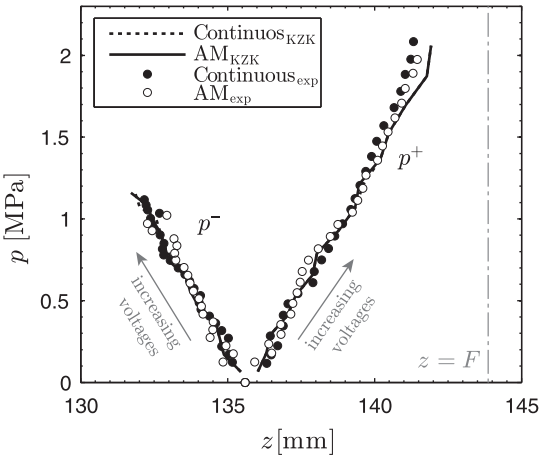


Fig. 3. On axis peak pressure location for both, continuous and 25 kHz-AM beams. Experimental and KZK solutions are shown. Location of the pressure maximum/minimum of experimental pulsed beam (black circles), experimental AM beam (open circles), simulated pulsed (continuous line) and AM beam (dashed line). The dashed-dotted vertical line represents the position of the geometric focus, $F=143.9$ mm.

3. Results

3.1. Maximum nonlinear focal shift in water

Fig. 3 shows the value and location of the on-axis peak compression and rarefaction pressures for 27 spaced initial excitation voltages at the source (between 5 V_p and 228 V_p). These particular points exhibit similar nonlinear shifts in the experiment and simulation for both continuous and 25 kHz-AM beams. The on-axis peak pressure position moves away from the transducer +5.8 mm for experimental data and 6.4 mm for simulated data. On the other hand, the on-axis peak rarefaction pressure position moves a maximum displacement of −4.0 mm towards the transducer in both cases. This focal displacements lead to a total difference between peak pressure and rarefaction focal positions of 9.8 mm for experimental measurements and 10.4 mm for the simulation results, which agree with the results reported in Camarena et al. [11] and Makov et al. [9] for a focused beam with a Fresnel number of 4.06. The agreement between experiments and simulations in the quasi-linear region (low and medium input voltages) is good, but they differ slightly at high power levels (nonlinear regime), the maximum pressure nonlinear focal shift effect being slightly higher in the simulation. A similar discrepancy was also detected in Camarena et al. [11] and was due to several causes: first, the frequency response of the hydrophone is bounded to 20 MHz, which limits the number of harmonics detected by the hydrophone. Second, the hydrophone response is only corrected by the magnitude of the frequency-dependent sensitivity in the range from 1 to 20 MHz. The lack of phase response for the deconvolution of the signals leads to uncertainties in the evaluation of the peak pressure. Finally, another possible source of error is due to the non-uniform vibration of the piezoelectric element, as discussed above. These hypotheses have been discussed in detail by Canney et al. [19].

In the case of the maximum intensity location (see Fig. 4), again the nonlinear shift is equal in both experiments with the continuous and the 25 kHz-AM beams. The intensity evaluated from Eq. (1) reaches a maximum at 80 W/cm^2 and suffers a shift of +1 mm both in the experiment and KZK simulation, which is quite small compared with the +5.8 mm displacement of the maximum pressure. Nevertheless, the ARF distribution (evaluated from Eq. (2)) undergoes a nonlinear shift that follows the same trend as pressure (compare Fig. 3 with Fig. 4), although the displacements of the maximum ARF are always slightly lower than those measured for pressure. A +4.6 mm ARF shift compared to +5.8 mm maximum pressure shift is reached in the highest nonlinear regime, i.e. 2.1 MPa peak pressure.

In order to understand the on-axis behavior of the particular points of the beam, a KZK simulation was performed in a range of excitation that covers from linear to strong nonlinear regime of propagation. Fig. 5 shows the on-axis location of the peak value for the pressure (p^+), each harmonic (numbered gray lines), intensity and ARF. In the linear regime, as intensity is proportional to the square of pressure and ARF is proportional to intensity, the three maximum matches and all the quantities peak at the same point. However, when a moderately nonlinear regime is reached, harmonics begin to appear (gray lines in Fig. 5). Because the nonlinear generation is progressive and cumulative, and since diffraction is lower at higher frequencies, the harmonics focus farther away than the fundamental, and each one does it further away than the previous one. Consequently, the peak of the total pressure moves away from the emitter. In this region, intensity also moves, but very slightly. The intensity of a nonlinear wave is the sum of the intensities of each harmonic, but as long as the main amplitude remains in the fundamental harmonic, it retains most of its energy, and consequently sets the position of the maximum intensity. The relevance of the fundamental is enhanced in the calculation of the intensity, because it is proportional to the square of the pressure. However, the same does not happen with the ARF, which is also

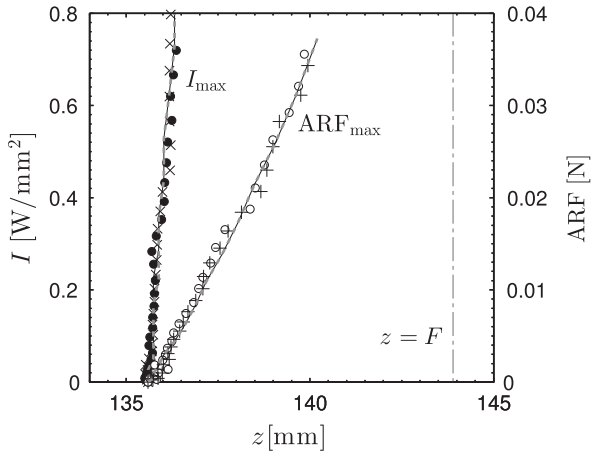


Fig. 4. On-axis maximum intensity position for continuous (×) and AM beams (black circles). Location of the on-axis ARF peak for continuous (+) and AM beams (white circles). Simulation curves are superimposed for continuous (continuous line) and AM beams (dashed lines). The dashed-dotted vertical line represents the position of the geometrical focus.

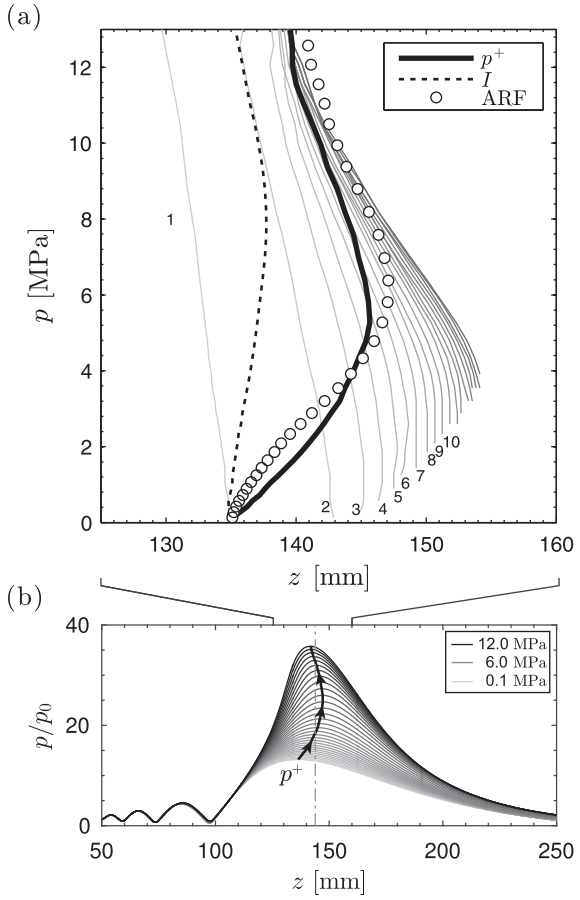


Fig. 5. (a) On-axis maximum pressure, p^+, intensity, I, and ARF location obtained from the KZK simulation of the ultrasonic beam in water. Numbered gray lines, represent the on-axis maximum pressure location of each harmonic. (b) Axial pressure profiles for increasing source amplitude, p_0 (increasing from gray to black). The thick black line shows the peak pressure location, p^+. The vertical dashed dotted line marks the geometrical focal.

proportional to the intensity of each harmonic, but corrected by the absorption coefficient, as shown in Eq. (4). In water, absorption increases with the square of the frequency, so the relevance of the harmonics is enhanced, the peak of the ARF moving significantly even in a moderately nonlinear regime. As we increase the initial excitation amplitude, of the emitter the number of harmonics in the propagation also increase, which can even make the ARF peak surpass the pressure peak. All these phenomena saturate (at around 6 MPa) and even retract at very high excitation levels because shock waves appear and nonlinear absorption drastically reduces the relevance of the harmonics. For this reason the peak locations of pressure, intensity and ARF move back to the emitter.

3.2. Dynamic nonlinear focal shift in water

The amplitude variation along the temporal profile of the 25 kHz-AM signal (see Fig. 6(a)) involves the coexistence of the linear regime propagation for periods with small amplitude (without distortion; see Fig. 6(b)) and the nonlinear regime propagation for the central periods (with large amplitude and distortion; see Fig. 6 (c)) during the propagation of the wave. This results in dynamic focal shifts during the application of the signal, as can be seen in Fig. 7 for the peak pressure, intensity and ARF.

These results show that the focusing characteristics of the beam can change in time when we modulate the excitation signal. Fig. 7 represents the highest excitation value reached in the experiment: 228 V_p in the transducer and a peak pressure of 2.02 MPa at the focus. The dynamic process proceeds as follows: first, the low amplitude cycles of the AM beam focus on a point around 136 mm from the source according to the medium properties and the source's physical characteristics: frequency, aperture, and geometrical focal length [9]. Then, as the local amplitude of the AM signal reaches nonlinear regime in the central part of the AM packet (see Fig. 6(c)), the focal maxima moves away from the source. At this point, the displacement reaches a maximum that perfectly agrees with the displacements shown previously in Figs. 3 and 4, and then returns toward the transducer, when the amplitude of the AM signal decreases. As shown, a different focal-shift behavior was obtained for pressure, ARF and intensity. The maximum focal displacement observed was +6.4 mm for positive pressure, −4 mm for rarefaction pressure, +1 mm for intensity and

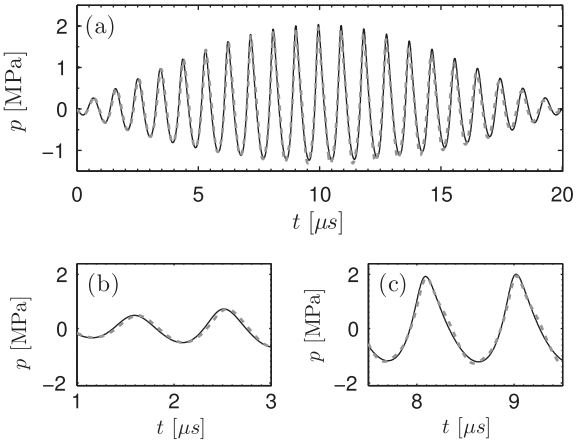


Fig. 6. Experimental (dashed line) and KZK simulated (continuous line) waveform measured at the focus for the 25-kHz AM beam. The input voltage in the experiment was 228 Vpp and the initial pressure in simulation was 105 kPa, chosen to produce equal pressure at the focus. (a) Complete half-period of the AM signal, where linear and nonlinear propagation coexist at different times. (b) Initial small-amplitude oscillations and (c) central oscillations of the AM signal, where strong nonlinearities are produced.

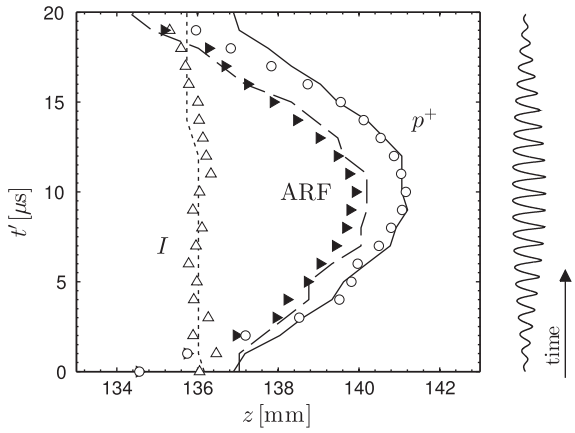


Fig. 7. On-axis simulated (lines) and experimental (markers) of the peak pressure (white circles), maximum intensity (white triangles) and maximum ARF (black triangles) locations obtained for each period of the AM-carrier component. t' is the dimensionless retarded time, where the time delay due to wave propagation distance has been eliminated.

+4.6 mm for the ARF. These results agree with the nonlinear focal shifts obtained in Section 3.2 for continuous beams.

As no shock waves were present in our experiment, we explored the strong nonlinear regime of propagation in an AM-modulated beam by means of a KZK simulation. Fig. 8 shows the nonlinear shift in two scenarios (moderate nonlinear regime: 2.02 MPa at the focus, which corresponds with the maximum excitation in our experiment) and 9.4 MPa at the focus (strong nonlinear regime).

The strong nonlinear scenario presents more complex dynamics than the moderate one. The maximum displacement of the focus was +12.5 mm for positive pressure, −8.1 mm for rarefaction pressure, +3.4 mm for intensity and +15.1 mm for ARF. The maximum position of the pressure exceeds the geometrical focus by

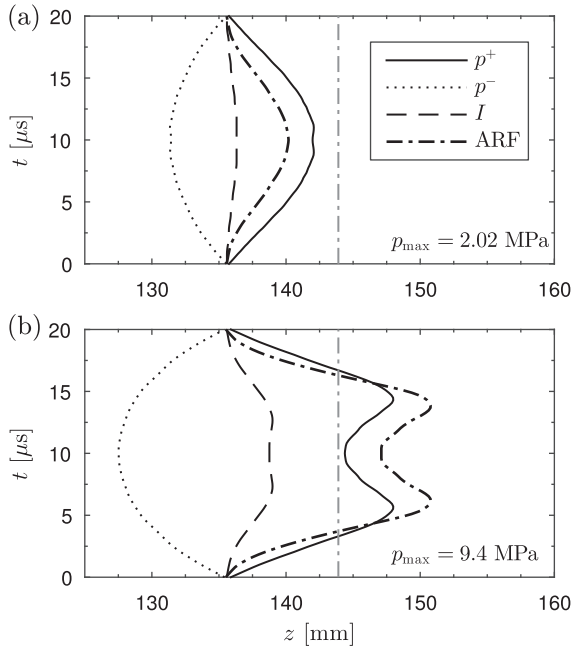


Fig. 8. On-axis dynamic focal displacements in water for a 25 kHz AM signal. Top: moderate nonlinear regime. Bottom: strong nonlinear regime. Peak pressure (solid line), rarefaction minimum (dashed line), intensity (dotted line) and ARF (dashed-dotted line). The vertical dashed line shows the geometric focus. (a) Weakly nonlinearity scenario, (b) strongly nonlinear scenario.

+4.2 mm, and the ARF one by +6.7 mm. However, when the signal amplitude is high enough to produce shock waves in the propagation, the focus returns to the transducer in both cases. This happens when the central part of the AM packet is propagating through the media, and is due to the effect of the nonlinear absorption associated with shock waves, which saturates the harmonic generation processes.

3.3. Dynamic nonlinear focal shift in liver

Multiple relaxation and inhomogeneities were introduced in the KZK model to simulate the propagation of the beam through a layer of soft-tissue (human liver). A set of seventy simulations were performed for amplitudes that ranged from the linear to strongly nonlinear regime. Fig. 9 shows the location of the peak pressure, each harmonic, intensity and ARF evaluated from Eq. (4). First, it can be observed that in the linear regime the focus is shifted towards the source due to the strong attenuation, where all the magnitudes peak at $z = 127.7$ mm (compared to 135.6 mm obtained in water). The linear position of the focus is located at 127.7 mm from the transducer, −8.3 mm before the focus obtained in water (136 mm). This effect is produced by the medium absorption in conjunction with an elongated focal area. Due to the high f-number of the source (2.57), the focal area, defined as the acoustic field area that exceeds 1/2 of the peak intensity, has an axial length of 45λ. During propagation through the focal area, where locally plane waves can be considered, the wave suffers from exponential decay. On this path a total attenuation of 3.2 dB is observed in tissue (considering 0.5 dB/cm/MHz the absorption of the liver [26]), so the peak pressure is located at the initial part of the focal area (127.7 mm) instead of at its location in weakly absorbing media such as water (136 mm). Despite this effect, in the weakly nonlinear regime ($p^+ < 2$ MPa) the nonlinear behavior of the peak pressure and intensity in soft-tissue is almost the same as in thermo-viscous media, in which each harmonic is progressively generated throughout the propagation and each one focus farther away than the previous one. However, the ARF shows a different behavior. ARF is also calculated by adding the intensities of the harmonics corrected each one by a factor proportional to its absorption. In soft-tissues the absorption follows a frequency power-law with an exponent $\gamma \approx 1$, (in contrast with thermo-viscous fluids where $\gamma = 2$). Therefore, as regards the ARF, higher harmonics have less relative importance to the fundamental one in tissue than in an equivalent thermoviscous media with $\gamma = 2$. Due to this, the observed focal shift of the ARF in human-liver is more relaxed than in water, as shown in Fig. 9. In the present case the ARF peak location falls between the maximum intensity and peak pressure location.

Then, in the moderately nonlinear regime ($2 < p^+ < 4$ MPa), it can be observed that the beam's self-defocusing effect grows with amplitude. The velocity of a finite amplitude perturbation depends on the wave amplitude, and for a focused beam the amplitude is higher along the propagation axis than in remote regions. Therefore, the compressive phases of the wave travel faster near the axis. Consequently, a flattening of the wave front is produced and a defocusing effect is observed: the pressure maximum is shifted from the source. The contrary effect is produced for the rarefaction phase of the waveform. Up to $p^+ < 6$ MPa, a total shift of +2.5 mm was observed for the intensity, while it was +9.4 mm for the peak pressure and +7.6 mm for the ARF. Note that these values are almost double those in water.

For higher amplitudes, the waveforms at the focal become strongly asymmetric: the compression region becomes sharper with high amplitude and the rarefaction region smoother with lower amplitude, as shown in Fig. 10. On the one hand, when these asymmetric shocks are present, the Rankine-Hugoniot jump conditions lead to an acceleration of the shock front near the axis in the focal area. As the shock-front speed increases, it becomes flattened. Again, the beam is self-refracted and this nonlinear self-action phenomena produces the de-focusing of the beam: the pressure maxima shifts. On the other hand, when shocks are present, nonlinear

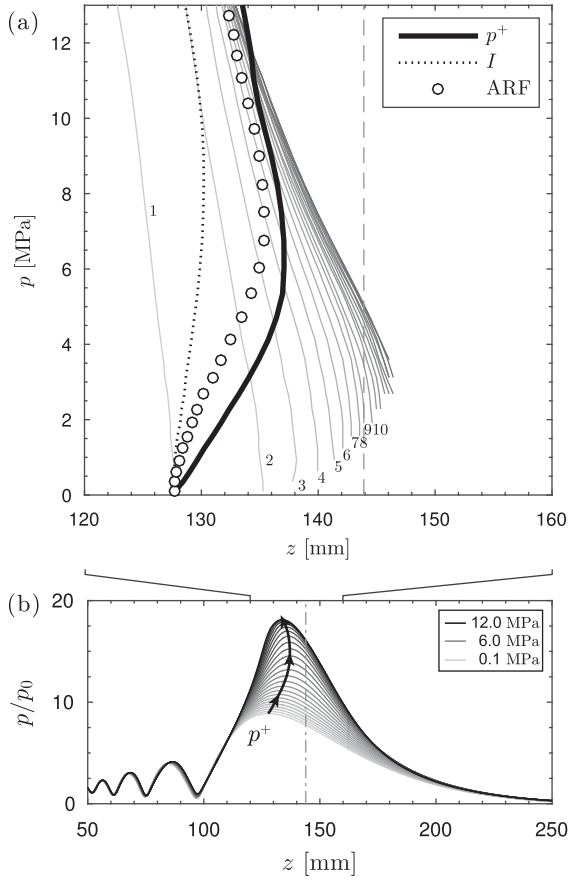


Fig. 9. (a) On-axis maximum pressure, p^+, intensity, $I+$, and ARF location obtained from the KZK simulation of the ultrasonic beam in tissue. Numbered gray lines represent the on-axis maximum pressure location of each harmonic. (b) Axial pressure profiles for increasing source amplitude, p_0 (increasing from gray to black). The thick black line shows the peak pressure location, p^+. The vertical dashed dotted line marks the geometrical focal.

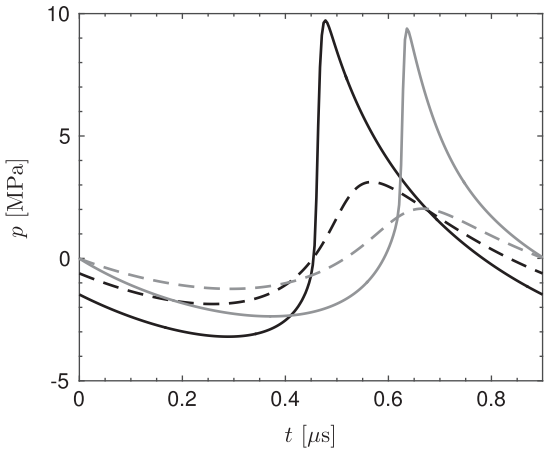


Fig. 10. Comparison of the waveforms captured at the peak pressure location in water (gray lines) and human liver tissue (black lines). Two excitation levels per media are shown, a moderately nonlinear scenario (2.9 MPa), and a strongly nonlinear scenario (9.5 MPa).

absorption is produced: the wave amplitude decreases sharply with distance. Therefore, it produces the opposite effect and the observed displacement of the peak pressure returns towards the source, as shown in Fig. 9 above $p^+ = 6$ MPa.

As before, 25 kHz-AM excitation signals were applied in two scenarios: moderate and strongly nonlinear propagation. The initial pressure values were chosen to produce similar pressure amplitudes at the focus as in the case of water: $p_0 = 0.26$ MPa amplitude excitation at the source surface, which leads to a peak pressure of $p^+ = 2.9$ MPa (moderate nonlinear scenario); and $p_0 = 0.69$ MPa on the transducer surface, which leads to a peak pressure of $p^+ = 9.5$ MPa (strongly nonlinear scenario). Waveforms captured at the peak pressure location are shown in Fig. 10 for both water and tissue simulations. Shock waves are formed for the highest amplitude calculations.

Fig. 11 shows the dynamic location of the on-axis positive pressure, minimum rarefaction and intensity maxima. In the moderate scenario, as shown in Fig. 11(a), the shifts are shorter than those obtained in water: +5.4 mm for peak pressure, −3.5 mm for peak negative pressure, +0.7 mm for intensity and +2.3 mm for the ARF, i.e., 15% lower for pressure, 30% for the intensity, and 50% for the ARF observed in water. The high value of the absorption in liver (0.5 dB/cm) compared to the absorption in water (0.002 dB/cm) drastically reduces the amplitude of the harmonics, and consequently the nonlinear shift effect.

Fig. 11(b) shows the dynamic nonlinear focal shift results for the strongly nonlinear scenario in human liver. A displacement of +9.3 mm for peak pressure is obtained, −7.1 mm for rarefaction pressure, +2.5 mm for intensity and +7.6 mm for the ARF. The maximum on-axis pressure location does not exceed the geometrical focus because the linear focus is closer to the emitter (127.7 mm) than in water, as explained above. In this case, the recoil in the shift is also observed in the central part of the AM packet, but is smaller than in water: the strong absorption in tissue makes it more difficult to generate shock waves in the pre-focal region.

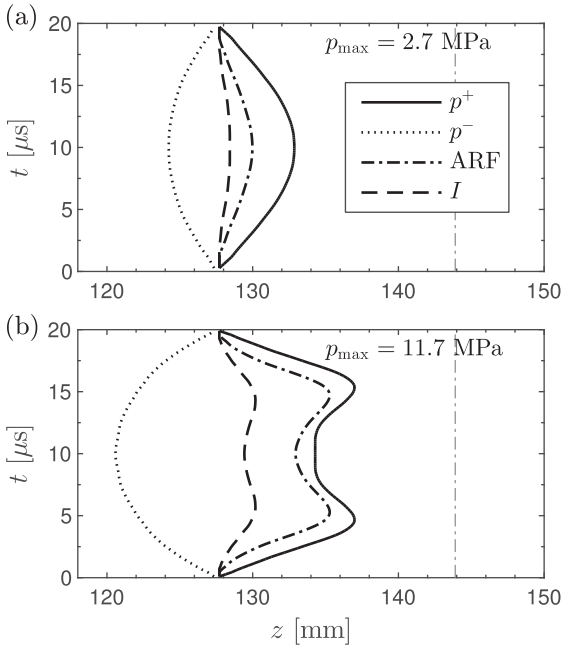


Fig. 11. On-axis focal displacements for a 25 kHz-AM beam in liver. Peak pressure (solid line), rarefaction minimum (dashed line), intensity (dotted line). The vertical dashed line shows the geometrical focus. (a) Weakly nonlinear scenario, (b) strongly nonlinear scenario.

4. Conclusions

This paper describes the analysis of the nonlinear behavior of the on-axis maximum pressure, intensity and ARF in a continuous and a 25 kHz AM beam (emitter characteristics: f-number = 2.6 and $f_0 = 1.112$ MHz). The pressure fields were measured in water and compared to those obtained from the numerical results based on the KZK equation, obtaining a good agreement between experimental and numerical data.

For a 25 kHz AM frequency, the maximum nonlinear shifts obtained in the AM beam match those obtained in the continuous beam, both in the linear and nonlinear regime; the on-axis peak pressure moves away from the transducer as the excitation in the emitter increases, while the rarefaction pressure moves in the opposite direction; intensity suffers a slight displacement and ARF moves away in an interval between the intensity shift and the positive pressure shift in the moderate nonlinear regime, and surpass the pressure shift in the strong nonlinear regime. Once the shock waves begin to appear, the nonlinear shifts begin to decrease. These entire phenomena have been explained in terms of harmonic generation and absorption during propagation in a lossy nonlinear medium both, for a continuous and an AM beam.

The results obtained demonstrate the ability of nonlinear AM beams generated with a mono-element transducer to produce dynamical axial focal displacements. The linear and nonlinear propagation regimes, together with shock waves and nonlinear absorption coexist during the semi-period of modulation of the beam (20 μs in our case). The same results, but with reduced magnitude, have been observed in a KZK simulation of the beam propagating in human liver.

Acoustic radiation force, and especially dynamic ARF, is widely used in many elasticity imaging techniques to induce displacements of tissue [15], or to remotely induce shear waves inside the medium [27]. We have observed that for amplitude-modulated beams, the position of maximum ARF changes with time, following the modulation function. Although the focusing degree of the devices used in these imaging techniques is considerably higher than the one considered in the present study, and as a consequence the nonlinear shift effects are lower in these image techniques, they can be important enough to affect the calculation of the elastic characteristic of the tissue. Future research will continue in this line. Finally, the phenomenology found in this work leads us to consider the possibility of exploring the generation of supersonic shear waves by means of a mono-element transducer excited by the appropriate amplitude-modulated signal: the frequency modulation would define the speed of the ARF displacement, while the maximum amplitude would fix the total distance covered.

Acknowledgements

FC acknowledge financial support from the AICO/2016-108 program of the Generalitat Valenciana. NJ acknowledge financial support from the FPI Grant PAID-2011 from the Universitat Politècnica de València. NGS acknowledge financial support from DPI2013-42236-R Project of the Spanish Ministry of Economy and Competitiveness, S2013/MIT-3024 of the Community of Madrid and from FPU Grant 12/02187 from the Spanish Ministry of Education, Culture and Sport.

References

[1] N. Bakhvalov, Y.M. Zhileikin, E. Zabolotskaya, R. Khokhlov, Focused high-amplitude sound beams, Sov. Phys. Acoust. 24 (1978) 10–15.
[2] B.G. Lucas, T.G. Muir, The field of a focusing source, J. Acoust. Soc. Am. 72 (1982) 1289–1296.

[3] F.A. Duck, H.C. Starritt, The locations of peak pressures and peak intensities in finite amplitude beams from a pulsed focused transducer, Ultrasound Med. Biol. 12 (1986) 403–409.
[4] J. Blitz, G. Simpson, Ultrasonic Methods of Non-destructive Testing, vol. 2, Springer Science & Business Media, London, 1995.
[5] F.A. Duck, A.C. Baker, H.C. Starritt, Ultrasound in Medicine, CRC Press, 1998.
[6] M. Hamilton, D. Blackstock, Nonlinear Acoustics, Academic Press, San Diego, CA 92101, USA, 1998.
[7] N. Bakhvalov, Y.M. Zhileikin, E. Zabolotskaya, Nonlinear propagation of sound beams with a uniform amplitude distribution, Sov. Phys. Acoust. 26 (1980) 95–100.
[8] M.A. Averkiou, M.F. Hamilton, Nonlinear distortion of short pulses radiated by plane and focused circular pistons, J. Acoust. Soc. Am. 102 (1997) 2539–2548.
[9] Y.N. Makov, V. Sánchez-Morcillo, F. Camarena, V. Espinosa, Nonlinear change of on-axis pressure and intensity maxima positions and its relation with the linear focal shift effect, Ultrasonics 48 (2008) 678–686.
[10] O. Bessonova, V. Khokhlova, M. Bailey, M. Canney, L. Crum, Focusing of high power ultrasound beams and limiting values of shock wave parameters, Acoust. Phys. 55 (2009) 463–473.
[11] F. Camarena, S. Adrián-Martínez, N. Jiménez, V. Sánchez-Morcillo, Nonlinear focal shift beyond the geometrical focus in moderately focused acoustic beams, J. Acoust. Soc. Am. 134 (2013) 1463–1472.
[12] J. Bercoff, M. Tanter, M. Fink, Supersonic shear imaging: a new technique for soft tissue elasticity mapping, IEEE Trans. Ultrason. Ferroelectr. Freq. Control 51 (2004) 396–409.
[13] T. Deffieux, E.E. Konofagou, Numerical study of a simple transcranial focused ultrasound system applied to blood-brain barrier opening, IEEE Trans. Ultrason. Ferroelectr. Freq. Control 57 (2010) 2637–2653.
[14] E. Lierke, T. Hemsel, Focusing cross-fire applicator for ultrasonic hyperthermia of tumors, Ultrasonics 44 (2006) e341–e344.
[15] C. Maleke, M. Pernot, E.E. Konofagou, Single-element focused ultrasound transducer method for harmonic motion imaging, Ultrason. Imaging 28 (2006) 144–158.
[16] D. Cathignol, O. Sapozhnikov, J. Zhang, Lamb waves in piezoelectric focused radiator as a reason for discrepancy between O'Neil's formula and experiment, J. Acoust. Soc. Am. 101 (1997) 1286–1297.
[17] H.T. O'Neil, Theory of focusing radiators, J. Acoust. Soc. Am. 21 (1949) 516–526.
[18] Y.-S. Lee, Numerical Solution of the KZK Equation for Pulsed Finite Amplitude Sound Beams in Thermoviscous Fluids, The University of Texas, Austin, 1993.
[19] M.S. Canney, M.R. Bailey, L.A. Crum, V.A. Khokhlova, O.A. Sapozhnikov, Acoustic characterization of high intensity focused ultrasound fields: a combined measurement and modeling approach, J. Acoust. Soc. Am. 124 (2008) 2406–2420.
[20] N. Bakhvalov, Y.M. Zhileikin, E.A. Zabolotskaya, Nonlinear Theory of Sound Beams, American Institute of Physics, New York, 1987.
[21] Y.A. Pishchalnikov, O.A. Sapozhnikov, T.V. Sinilo, Increase in the efficiency of the shear wave generation in gelatin due to the nonlinear absorption of a focused ultrasonic beam, Acoust. Phys. 48 (2002) 214–219.
[22] O. Rudenko, A. Sarvazyan, S.Y. Emelianov, Acoustic radiation force and streaming induced by focused nonlinear ultrasound in a dissipative medium, J. Acoust. Soc. Am. 99 (1996) 2791–2798.
[23] A.P. Sarvazyan, O.V. Rudenko, W.L. Nyborg, Biomedical applications of radiation force of ultrasound: historical roots and physical basis, Ultrasound Med. Biol. 36 (2010) 1379–1394.
[24] B.B. Guzina, E.V. Dontsov, M.W. Urban, M. Fatemi, The "sixth sense" of ultrasound: probing nonlinear elasticity with acoustic radiation force, Phys. Med. Biol. 60 (2015) 3775.
[25] X. Yang, R.O. Cleveland, Time domain simulation of nonlinear acoustic beams generated by rectangular pistons with application to harmonic imaging, J. Acoust. Soc. Am. 117 (2005) 113–123.
[26] Y. Fujii, N. Taniguchi, K. Itoh, K. Shigeta, Y. Wang, J.-W. Tsao, K. Kumasaki, T. Itoh, A new method for attenuation coefficient measurement in the liver comparison with the spectral shift central frequency method, J. Ultrasound Med. 21 (2002) 783–788.
[27] K.R. Nightingale, M.L. Palmeri, R.W. Nightingale, G.E. Trahey, On the feasibility of remote palpation using acoustic radiation force, J. Acoust. Soc. Am. 110 (2001) 625–634.